

Comparative study on modal identification methods using output-only information

Jin-Hak Yi[†]

*Smart Infra-Structure Technology Center, Korea Advanced Institute of Science and Technology,
Daejeon 305-701, Korea*

Chung-Bang Yun[‡]

*Department of Civil and Environmental Engineering, Korea Advanced Institute of Science and Technology,
Daejeon 305-701, Korea*

(Received March 12, 2003, Accepted January 7, 2004)

Abstract. In this paper, several modal identification techniques for output-only structural systems are extensively investigated. The methods considered are the power spectral method, the frequency domain decomposition method, the Ibrahim time domain method, the eigensystem realization algorithm, and the stochastic subspace identification method. Generally, the power spectral method is most widely used in practical area, however, the other methods may give better estimates particularly for the cases with closed modes and/or with large measurement noise. Example analyses were carried out on typical structural systems under three different loading cases, and the identification performances were examined through the comparisons between the estimates by various methods.

Key words: modal identification; output-only information; power spectral method; frequency domain decomposition; Ibrahim time domain; eigensystem realization algorithm; stochastic subspace identification.

1. Introduction

Experimental modal testing and analysis are gaining more attention for monitoring and structural integrity assessment of civil infrastructures such as bridges and buildings. For example, forced vibration tests are frequently carried out to identify the modal properties of newly built long span bridges, and the results are used to verify the finite element models and to establish the baseline properties for the integrity assessments in the future.

Vibration tests are generally classified as the forced vibration tests (FVTs) and the ambient vibration tests (AVTs). AVTs may be performed under normal operating conditions with uncontrollable and immeasurable ambient loads such as traffic and wind loadings, while FVTs just can be carried out using the controllable and/or measurable loads applied by droppers and shakers. FVTs usually require much more expensive equipments and controlled operating conditions.

[†] Research Assistant Professor

[‡] Professor

However, AVTs may be carried out under normal operating conditions and require simpler equipments. From this point of view, AVTs may be considered as more preferable testing methods for large infrastructures such as bridges, buildings, and dams. The non-stationarity in ambient loads would be one obstacle to apply AVTs to modal testing; however, the undesirable non-stationary effect can be minimized by collecting a sufficiently long data or deleting any parts of the response data under the non-stationary ambient loads.

There are several modal identification techniques using output-only information. The most general method in engineering field might be the power spectral method in which the modal parameters can be identified by reading the peak frequencies and the amplitude of the power spectral density functions (Newland 1984, Bendat and Piersol 1993). Recently, the frequency domain decomposition method was developed using the singular value decomposition of the power spectral density function matrix (Otte *et al.* 1990, Brinker *et al.* 2000). The power spectral method and the frequency domain decomposition method are performed in the frequency domain. On the other hands there are several time domain methods developed using an assumption that the ambient loads are Gaussian white noise processes. Ibrahim time domain method was developed in late 1970s (Ibrahim and Mikulcik 1977, Ibrahim and Pappa 1982), which was formulated based on the condition with free vibration responses in continuous time domain. The eigensystem realization algorithm (Juang and Pappa 1985, Juang 1994) and the stochastic subspace identification method (Hermans and Van Der Auweraer 1990, Overschee and De Moor 1996) were developed based on the system theory in the discrete time domain.

In this paper, the above-mentioned techniques are briefly summarized and their performances are investigated through the extensive comparative studies for three example cases. The first example is the ASCE benchmark model of a 2-bay and 4-story building provided by the ASCE benchmark task group on structural health monitoring and damage detection (ASCE 2000, Johnson *et al.* 2000). The second one is a 5-story steel frame tested on a shaking table in National Taiwan University (NTU) (Loh *et al.* 2000). The last one is a scaled bridge model tested in Korea Institute of Machinery and Materials (KIMM) (Lee *et al.* 2002). They are subjected to three different types of ambient loads: i.e. random excitations of a long duration at the roof for the ASCE model, earthquake loads for the NTU structure and vehicle loads for the bridge model. These three example cases cover two typical structural systems subjected to ambient loads frequently encountered. The case with the ASCE model is a numerical simulation study, and several levels of the noise are imposed on the measured data. Then the relationship between the intensity of the measurement noise and the identification results are extensively investigated. In the case of the NTU structure, the experiments are carried out for two different earthquake ground motions with different frequency components, and the consistency between the estimates is examined. In the case of the bridge model, 10 times of the vehicles tests are carried out, and the consistency of the estimates for 10 different cases by each identification method is intensively investigated.

2. Revisits to modal parameter identification

2.1 Power spectral method

In the power spectral (PS) method, the modal parameters can be estimated by reading the peak frequencies and peak amplitudes of the power spectral density (PSD) functions of the structural

response data. Therefore this method is also addressed as the peak picking method, or the direct reading method. Natural frequencies can be determined as the peak frequencies and the mode shapes can be obtained using the ratios of the PSD functions at the corresponding peak frequencies as follows

$$\phi_{ak} = \frac{S_{y_a y_b}(\omega_k)}{S_{y_b y_b}(\omega_k)}, \quad \boldsymbol{\varphi}_k = \{\phi_{1k} \ \phi_{2k} \ \dots \ \phi_{N_m k}\}^T \quad (1)$$

where, ϕ_{ak} is the k -th mode shape component at Point a , ω_k is the k -th natural frequency, and $S_{y_a y_b}$ and $S_{y_b y_b}$ are the PSD functions of the measurement data at Points a and b with respect to the reference Point b . N_m is the number of the measured DOFs.

2.2 Frequency domain decomposition method

In the frequency domain decomposition (FDD) method (Otte *et al.* 1990, Brinker 2000), the singular values of the PSD function matrix $\mathbf{S}_{yy}(\omega)$ are used to estimate the natural frequencies instead of the PSD functions themselves as follows

$$\mathbf{S}_{yy}(\omega) = \mathbf{U}(\omega)^T \boldsymbol{\Sigma}(\omega) \mathbf{V}(\omega) \quad (2)$$

where $\boldsymbol{\Sigma}$ is the diagonal matrix consisting of the singular values (σ_i 's) and \mathbf{U} and \mathbf{V} are unitary matrices. Since $\mathbf{S}_{yy}(\omega)$ is symmetric, \mathbf{U} becomes equal to \mathbf{V} . In this FDD method, the natural frequencies can be determined from the peak frequencies of the singular values, and the mode shape from anyone of the column vectors of $\mathbf{U}(\omega)$ at the corresponding peak frequencies. Generally the first singular value $\sigma_1(\omega)$ among σ_i 's ($i = 1, \dots, N$) is used to estimate the modal parameters except in some special cases such as with two or more identical excitations.

2.3 Ibrahim time domain method

The Ibrahim time domain (ITD) method (Ibrahim and Mikulcik 1977, Ibrahim and Pappa 1982) was developed to deal with the free vibration responses. When the ambient loads are Gaussian random processes of white noises or wide-band processes, the free vibration responses can be extracted using the random decremental technique (Ibrahim 1977, Yang *et al.* 1984) or the cross-correlation functions (James *et al.* 1996, Yam *et al.* 1997). In this study, the cross-correlation functions are used to obtain the free vibration signatures. Then the ITD method can be applied thereafter.

The free vibration responses can be expressed using the complex mode shapes ($\boldsymbol{\varphi}_k \in \mathbb{R}^{N_m \times 1}$) and eigenvalues (λ_k) as follows

$$\mathbf{y}(t) = \sum_{k=1}^N \boldsymbol{\varphi}_k e^{\lambda_k t} \quad (3)$$

where N_m is the number of measured points, N is the number of the modes to be extracted, and $\boldsymbol{\varphi}_k$ and λ_k are the complex mode shape and eigenvalue for the k -th mode, respectively. In this study, the free vibration responses $\mathbf{y}(t)$ are obtained using the cross-correlation functions of the measured ambient responses. From Eq. (3), the following response matrices \mathbf{Y} and $\hat{\mathbf{Y}}$ consisting of the free vibration response data can be constructed as

$$\mathbf{Y} = [\mathbf{y}(t) \ \dots \ \mathbf{y}(t + (N_{ITD} - 1)\Delta t)] = [\boldsymbol{\varphi}_1 \ \dots \ \boldsymbol{\varphi}_N] \begin{bmatrix} e^{\lambda_1 t} & \dots & e^{\lambda_1(t + (N_{ITD} - 1)\Delta t)} \\ \vdots & \ddots & \vdots \\ e^{\lambda_N t} & \dots & e^{\lambda_N(t + (N_{ITD} - 1)\Delta t)} \end{bmatrix} \quad (4)$$

$$\hat{\mathbf{Y}} = [\mathbf{y}(t + \Delta t) \ \dots \ \mathbf{y}(t + N_{ITD}\Delta t)] = [\boldsymbol{\varphi}_1 \ \dots \ \boldsymbol{\varphi}_N] \begin{bmatrix} e^{\lambda_1\Delta t} & \dots & 0 \\ \vdots & \ddots & \vdots \\ 0 & \dots & e^{\lambda_N\Delta t} \end{bmatrix} \begin{bmatrix} e^{\lambda_1 t} & \dots & e^{\lambda_1(t + (N_{ITD} - 1)\Delta t)} \\ \vdots & \ddots & \vdots \\ e^{\lambda_N t} & \dots & e^{\lambda_N(t + (N_{ITD} - 1)\Delta t)} \end{bmatrix} \quad (5)$$

where N_{ITD} is the number of response data used for the ITD method. Then a system matrix $\mathbf{A}^{ITD} (\in \mathbf{R}^{N_m \times N_m})$ may be defined from the relationship between \mathbf{Y} and $\hat{\mathbf{Y}}$ as

$$\mathbf{A}^{ITD} \mathbf{Y} = \hat{\mathbf{Y}} \quad (6)$$

$$\mathbf{A}^{ITD} = (\hat{\mathbf{Y}} \mathbf{Y}^T) (\mathbf{Y} \mathbf{Y}^T)^{-1} \quad (7)$$

Then, from Eqs. (4)-(6), the following equation can be obtained, which defines an eigenvalue problem of a system matrix \mathbf{A}^{ITD} as follows

$$\mathbf{A}^{ITD} \boldsymbol{\Phi} = \boldsymbol{\Phi} \begin{bmatrix} e^{\lambda_1\Delta t} & \dots & 0 \\ \vdots & \ddots & \vdots \\ 0 & \dots & e^{\lambda_N\Delta t} \end{bmatrix} \quad (8)$$

where, $\boldsymbol{\Phi} = [\boldsymbol{\varphi}_1 \ \boldsymbol{\varphi}_2 \ \dots \ \boldsymbol{\varphi}_N]$. Since \mathbf{A}^{ITD} is a real matrix, the eigenvalues and vectors can be obtained as pairs of complex conjugates. Then the natural frequency ω_k and modal damping ratio ξ_k can be determined as

$$\begin{aligned} \lambda_k &= \frac{1}{\Delta t} \ln(\mu_k) \\ \xi_k &= -\text{Re}(\lambda_k)/|\lambda_k| \\ \omega_k &= -\text{Im}(\lambda_k)/\sqrt{1 - \xi_k^2} \end{aligned} \quad (9)$$

The complex mode shapes are transformed to minimize the imaginary part and then the real parts of the transformed complex mode shape are taken as the structural mode shapes.

2.4 Eigensystem realization algorithm

The eigensystem realization algorithm (ERA) was also developed to deal with the free vibration response (Juang and Pappa 1985, Juang 1994). It is based on the discrete state space equation of structural system as

$$\begin{aligned} \mathbf{z}(k+1) &= \mathbf{A}\mathbf{z}(k) + \mathbf{B}\mathbf{u}(k) & (\mathbf{z}(k), \mathbf{z}(k+1) \in \mathbf{R}^{N \times 1}, \mathbf{u}(k) \in \mathbf{R}^{N_u \times 1}, \mathbf{A} \in \mathbf{R}^{N \times N}, \mathbf{B} \in \mathbf{R}^{N \times N_u}) \\ \mathbf{y}(k) &= \mathbf{C}\mathbf{z}(k) & (\mathbf{y}(k) \in \mathbf{R}^{N_m \times 1}, \mathbf{C} \in \mathbf{R}^{N_m \times N}) \end{aligned} \quad (10)$$

where \mathbf{z} , \mathbf{u} , and \mathbf{y} are the state vector, external load vector and observation vector, respectively; and matrices \mathbf{A} , \mathbf{B} , and \mathbf{C} are the system matrices; and N_u is the number of external loads. For a case of free vibration with an impulsive excitation at the beginning: i.e., $\mathbf{u}(0) = \mathbf{1}$ and $\mathbf{u}(k) = \mathbf{0}$ ($k = 1, 2, \dots$), the observation vector $\mathbf{y}(k)$ can be obtained as a Markov process as

$$\mathbf{y}(k) = \mathbf{CA}^{k-1}\mathbf{B} \quad (11)$$

In this study, the free vibration responses $\mathbf{y}(k)$ are obtained using the correlation functions of the ambient responses as in the ITD method. Constructing the block Hankel matrix $\mathbf{H}_{n_1, n_2}^{ERA} \in \mathbf{R}^{N_m n_1 \times n_2}$ with the observed data $\mathbf{y}(k)$, the block Hankel matrix can be decomposed into the observability matrix $\mathcal{O}_{n_1} \in \mathbf{R}^{N_m n_1 \times n_2}$, the system matrix \mathbf{A} and the controllability matrix $\mathcal{C}_{n_2} \in \mathbf{R}^{N_m \times n_2}$ from the last equality of the Eq. (12).

$$\begin{aligned} \mathbf{H}_{n_1, n_2}^{ERA}(k-1) &= \begin{bmatrix} \mathbf{y}(k) & \dots & \mathbf{y}(k+t_{n_2-1}) \\ \vdots & \ddots & \vdots \\ \mathbf{y}(j_{n_1-1}+k) & \dots & \mathbf{y}(j_{n_1-1}+k+t_{n_2-1}) \end{bmatrix} \\ &= \begin{bmatrix} \mathbf{C} \\ \vdots \\ \mathbf{CA}^{j_{n_1-1}} \end{bmatrix} \mathbf{A}^{k-1} [\mathbf{B} \ \dots \ \mathbf{A}^{t_{n_2-1}} \mathbf{B}] = \mathcal{O}_{n_1} \mathbf{A}^{k-1} \mathcal{C}_{n_2} \end{aligned} \quad (12)$$

$$\text{where } \mathcal{O}_{n_1} = \begin{bmatrix} \mathbf{C} \\ \vdots \\ \mathbf{CA}^{j_{n_1-1}} \end{bmatrix}, \quad \mathcal{C}_{n_2} = [\mathbf{B} \ \dots \ \mathbf{A}^{t_{n_2-1}} \mathbf{B}]$$

where j_i ($i = 1, \dots, n_1$) and t_i ($i = 1, \dots, n_2$) are the random integers, and the ERA method may be equal to the Ho-Kalman algorithm if j_i and t_i are set as sequential integers (Ho and Kalman 1966). In the ERA method, the block Hankel matrix $\mathbf{H}_{n_1, n_2}^{ERA}(0)$ at $k=0$ are decomposed into unitary matrices \mathbf{U}_1 and \mathbf{V}_1 and singular value matrix Σ_1 using the minimum order realization concept (Juang and Pappa 1985) as follows

$$\begin{aligned} \mathbf{H}_{n_1, n_2}^{ERA}(0) &= \mathbf{U}\Sigma\mathbf{V}^T = [\mathbf{U}_1 \ \mathbf{U}_2] \begin{bmatrix} \Sigma_1 & \mathbf{0} \\ \mathbf{0} & \Sigma_2 \end{bmatrix} \begin{bmatrix} \mathbf{V}_1 \\ \mathbf{V}_2 \end{bmatrix} \\ &= \mathbf{U}_1 \Sigma_1 \mathbf{V}_1^T + \mathbf{U}_2 \Sigma_2 \mathbf{V}_2^T \approx \mathbf{U}_1 \Sigma_1 \mathbf{V}_1^T \end{aligned} \quad (13)$$

The size of the singular value matrix Σ_1 can be determined by considering the condition that $\min(\text{diag}(\Sigma_1)) > \max(\text{diag}(\Sigma_2)) \approx 0$ or by using the stabilization chart introduced in Section 2.6. From the Eqs. (12) and (13), the term $\mathbf{H}_{n_1, n_2}^{ERA}(k)$ can be expressed as (Juang and Pappa 1985),

$$\mathbf{H}_{n_1, n_2}^{ERA}(k) = \mathbf{U}_1 \boldsymbol{\Sigma}_1^{1/2} [\boldsymbol{\Sigma}_1^{-1/2} \mathbf{U}_1^T \mathbf{H}_{n_1, n_2}^{ERA}(1) \mathbf{V}_1 \boldsymbol{\Sigma}_1^{-1/2}]^k \boldsymbol{\Sigma}_1^{1/2} \mathbf{V}_1^T \quad (14)$$

and $\mathbf{y}(k+1)$ can be also obtained by taking the first block of the $\mathbf{H}_{n_1, n_2}^{ERA}(k)$ as

$$\begin{aligned} \mathbf{y}(k+1) &= \mathbf{E}_{n_1}^T \mathbf{H}_{n_1, n_2}^{ERA}(k) \mathbf{E}_{n_2} \\ &= \mathbf{E}_{n_1}^T \mathbf{U}_1 \boldsymbol{\Sigma}_1^{1/2} [\boldsymbol{\Sigma}_1^{-1/2} \mathbf{U}_1^T \mathbf{H}_{n_1, n_2}^{ERA}(1) \mathbf{V}_1 \boldsymbol{\Sigma}_1^{-1/2}]^k \boldsymbol{\Sigma}_1^{1/2} \mathbf{V}_1^T \mathbf{E}_{n_2} \end{aligned} \quad (15)$$

where $\mathbf{E}_{n_1}^T = [\mathbf{I}_{n_1}, \mathbf{0}_{n_1}, \dots, \mathbf{0}_{n_1}]$ and $\mathbf{E}_{n_2}^T = [\mathbf{I}_{n_2}, \mathbf{0}_{n_2}, \dots, \mathbf{0}_{n_2}]$. From the Eqs. (11) and (15), the system matrices \mathbf{A} , \mathbf{B} and \mathbf{C} can be obtained using \mathbf{U}_1 , $\boldsymbol{\Sigma}_1$, and \mathbf{V}_1 ; i.e. the results of the SVD of $\mathbf{H}_{n_1, n_2}^{ERA}(0)$ and $\mathbf{H}_{n_1, n_2}^{ERA}(1)$ as follows

$$\begin{aligned} \mathbf{A} &= \boldsymbol{\Sigma}_1^{-1/2} \mathbf{U}_1^T \mathbf{H}_{n_1, n_2}^{ERA}(1) \mathbf{V}_1 \boldsymbol{\Sigma}_1^{-1/2} \\ \mathbf{B} &= \boldsymbol{\Sigma}_1^{1/2} \mathbf{V}_1^T \mathbf{E}_{n_2} \\ \mathbf{C} &= \mathbf{E}_{n_1}^T \mathbf{U}_1 \boldsymbol{\Sigma}_1^{1/2} \end{aligned} \quad (16)$$

The eigenvalues and vectors of the discrete system can be calculated from eigenvalue decomposition of system matrix \mathbf{A} that is similar to Eq. (8).

$$\mathbf{A}\Psi = \Psi\mathbf{M} \quad (\mathbf{M} = diag(\mu_1, \dots, \mu_N) \in \mathbf{R}^{N \times N} \text{ and } \Psi = [\Psi_1 \dots \Psi_N] \in \mathbf{R}^{N \times N}) \quad (17)$$

Finally, the eigenvalue, modal damping ratio, natural frequency and modal vector for the physical system can be obtained as follows

$$\begin{aligned} \lambda_k &= \frac{1}{\Delta t} \ln \mu_k \\ \xi_k &= -\text{Re}(\lambda_k) / |\lambda_k| \\ \omega_k &= -\text{Im}(\lambda_k) / \sqrt{1 - \xi_k^2} \\ \boldsymbol{\varphi}_k &= \mathbf{C} \boldsymbol{\psi}_k \end{aligned} \quad (18)$$

2.5 Stochastic subspace identification method

The stochastic subspace identification (SSI) method utilizes the SVD of a block Hankel matrix with cross correlation matrix of responses, and there are two kinds of the SSI methods; one is SSI/BR (balanced realization) and the other is SSI/CVA (canonical variate analysis). The fundamental base for this method is the stochastic state space equation, which considers the system dynamics under the stochastic random excitation or random noises as

$$\begin{aligned} \mathbf{z}(k+1) &= \mathbf{A}\mathbf{z}(k) + \mathbf{w}(k) \\ \mathbf{y}(k) &= \mathbf{C}\mathbf{z}(k) + \mathbf{v}(k) \end{aligned} \quad (19)$$

where $\mathbf{w}(k)$ and $\mathbf{v}(k)$ are statistically uncorrelated white noise vector sequences with zero means representing the process and measurement noises, respectively. Then, the cross correlation function $\mathbf{R}(k)$ can be calculated using the Eq. (19)

$$\mathbf{R}(k) = E[\mathbf{y}(k+m)\mathbf{y}(m)^T] = \mathbf{C}\mathbf{A}^{k-1}E[\mathbf{z}(m+1)\mathbf{y}(m)^T] = \mathbf{C}\mathbf{A}^{k-1}\mathbf{G} \quad (20)$$

where $\mathbf{G} \triangleq E[\mathbf{z}(m+1)\mathbf{y}(m)^T]$. Constructing the block Hankel matrix with the cross correlation matrix, this block Hankel matrix can be decomposed into an observability matrix and an extended controllability matrix as in the last equality of Eq. (21)

$$\begin{aligned} \mathbf{H}_{n_1, n_2}^{SSI} &= \begin{bmatrix} \mathbf{R}_1 & \dots & \mathbf{R}_{n_2} \\ \vdots & \ddots & \vdots \\ \mathbf{R}_{n_1} & \dots & \mathbf{R}_{n_1+n_2-1} \end{bmatrix} = \begin{bmatrix} \mathbf{C}\mathbf{G} & \dots & \mathbf{C}\mathbf{A}^{n_2-1}\mathbf{G} \\ \vdots & \ddots & \vdots \\ \mathbf{C}\mathbf{A}^{n_1-1}\mathbf{G} & \dots & \mathbf{C}\mathbf{A}^{n_1+n_2-2}\mathbf{G} \end{bmatrix} \\ &= \begin{bmatrix} \mathbf{C} \\ \vdots \\ \mathbf{C}\mathbf{A}^{n_1-1} \end{bmatrix} [\mathbf{G} \ \dots \ \mathbf{A}^{n_2-1}\mathbf{G}] = \mathcal{O}_{n_1} \mathcal{C}_{n_2}^{ext} \\ \text{where } \mathcal{O}_{n_1} &\triangleq \begin{bmatrix} \mathbf{C} \\ \vdots \\ \mathbf{C}\mathbf{A}^{n_1-1} \end{bmatrix}, \quad \mathcal{C}_{n_2}^{ext} \triangleq [\mathbf{G} \ \dots \ \mathbf{A}^{n_2-1}\mathbf{G}] \end{aligned} \quad (21)$$

After pre- and post-multiplying of invertible weighting matrices \mathbf{W}_1 and \mathbf{W}_2 , respectively, to the block Hankel matrix $\mathbf{H}_{n_1, n_2}^{SSI}$ and by decomposing it into $\mathbf{W}_1\mathcal{O}_{n_1}$ and $\mathcal{C}_{n_2}^{ext}\mathbf{W}_2$, the observability matrix \mathcal{O}_{n_1} can be obtained as follows

$$\begin{aligned} \mathbf{W}_1 \mathbf{H}_{n_1, n_2}^{SSI} \mathbf{W}_2 &= [\mathbf{U}_1 \ \mathbf{U}_2] \begin{bmatrix} \Sigma_1 & \mathbf{0} \\ \mathbf{0} & \mathbf{0} \end{bmatrix} \begin{bmatrix} \mathbf{V}_1^T \\ \mathbf{V}_2^T \end{bmatrix} \approx \mathbf{U}_1 \Sigma_1 \mathbf{V}_1^T \Leftrightarrow \mathbf{W}_1 \mathcal{O}_{n_1} \mathcal{C}_{n_2}^{ext} \mathbf{W}_2 \\ \therefore \mathcal{O}_{n_1} &= \mathbf{W}_1^{-1} \mathbf{U}_1 \Sigma_1^{1/2} \end{aligned} \quad (22)$$

Finally, the system matrix \mathbf{A} can be obtained using the upper $(n_1 - 1)$ block matrix deleting the last block row of \mathcal{O}_{n_1} and lower $(n_1 - 1)$ block matrix of the upper-shifted matrix by one block row as

$$\begin{aligned} \mathcal{O}_{n_1-1}^\uparrow &= \mathcal{O}_{n_1-1} \mathbf{A} \\ \text{where } \mathcal{O}_{n_1-1}^\uparrow &\triangleq \begin{bmatrix} \mathbf{C}\mathbf{A} \\ \mathbf{C}\mathbf{A}^2 \\ \vdots \\ \mathbf{C}\mathbf{A}^{n_1-1} \end{bmatrix}, \quad \mathcal{O}_{n_1-1} \triangleq \begin{bmatrix} \mathbf{C} \\ \mathbf{C}\mathbf{A} \\ \vdots \\ \mathbf{C}\mathbf{A}^{n_1-2} \end{bmatrix} \end{aligned} \quad (23)$$

Two kinds of the SSI method can be derived according to the way of choosing the weighting matrices. The first is the SSI/BR (balanced realization) by using identity matrices as the weighting matrices. The second is the SSI/CVA (canonical variate analysis) by using the matrices in Eq. (24) as the weighting matrices, which were obtained by maximizing the correlation between the measured time history data at different locations (Hermans *et al.* 1999).

$$\mathbf{W}_1 = \mathbf{L}^{+1}, \quad \mathbf{W}_2 = \mathbf{L}^{-1}$$

where $\mathcal{R}^+ = \begin{bmatrix} \mathbf{R}_0 & \dots & \mathbf{R}_{p-1}^T \\ \vdots & \ddots & \vdots \\ \mathbf{R}_{p-1} & \dots & \mathbf{R}_0 \end{bmatrix} = \mathbf{L}^+ \mathbf{L}^{+T}, \quad \mathcal{R}^- = \begin{bmatrix} \mathbf{R}_0 & \dots & \mathbf{R}_{q-1}^T \\ \vdots & \ddots & \vdots \\ \mathbf{R}_{q-1} & \dots & \mathbf{R}_0 \end{bmatrix} = \mathbf{L}^- \mathbf{L}^{-T}$ (24)

2.6 Construction of stabilization chart

In the cases of time domain identification techniques such as ERA and SSI, an appropriate system order should be determined. In the case of a structural model with n-DOFs, the size of system matrix \mathbf{A} is certainly $2n$ because the state vector consists of the displacements and velocities. However, a structure generally has infinite number of DOFs. So the meaningful system order should be determined to carry out engineering problems. If a structure can be reasonably represented as a system with n-DOFs, the following relationship can be obtained for the singular values as

$$\sigma_1 \geq \sigma_2 \geq \dots \geq \sigma_{2n} \gg \sigma_{2n+1} \geq \sigma_{2n+2} \geq \dots \geq 0 \quad (25)$$

Therefore, it would be possible to find out the suitable system order by looking into the trend of singular values. But in reality, it may be very difficult to find out a large drop in singular values due to the effect of the measurement noise. In such cases, the proper system order may be determined by looking into the trend of the estimated modal parameters in a stabilization chart (as shown in Section 3.1.3), as the system order increases sequentially. The following criteria can be used to classify a mode as stable mode, unstable mode, and noise mode. If the estimated modal damping ratio is larger than a prescribed value as in Eq. (26), this mode is classified as a noise mode,

$$\xi_j^{(p)} > \xi_{noise_cr} \quad (26)$$

where $\xi_j^{(p)}$ is j -th identified modal damping ratio at the system order p , and ξ_{noise_cr} is the prescribed critical value for damping ratio. Among the non-noise modes, those satisfying Eqs. (27)-(29) can be classified as stable modes. Otherwise, they may be considered as unstable modes.

$$\frac{f_j^{(p)} - f_j^{(p+1)}}{f_j^{(p)}} < \Delta f_{stable_cr} \quad (27)$$

$$\frac{\xi_j^{(p)} - \xi_j^{(p+1)}}{\xi_j^{(p)}} < \Delta \xi_{stable_cr} \quad (28)$$

$$1 - \frac{\|\boldsymbol{\phi}_j^{(p)} \cdot \boldsymbol{\phi}_j^{(p+1)}\|^2}{\|\boldsymbol{\phi}_j^{(p)}\|^2 \|\boldsymbol{\phi}_j^{(p+1)}\|^2} < \Delta \phi_{stable_cr} \quad (29)$$

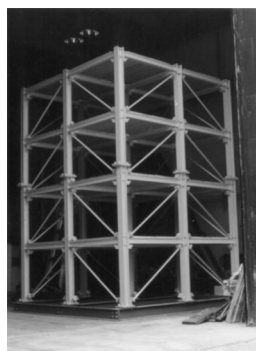
where, $f_j^{(p)}$ and $\phi_j^{(p)}$ are j -th natural frequency and mode shape at the system order p , respectively, and, Δf_{stable_cr} , $\Delta \xi_{stable_cr}$, and $\Delta \phi_{stable_cr}$ are the tolerance values for the natural frequency, damping ratio, and mode shape. The tolerance values may be determined by considering the structural type and the confidence level of the measurement data.

3. Example analyses

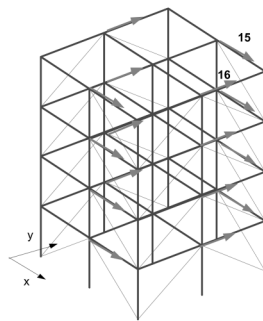
3.1 Example 1: ASCE benchmark structure subjected to roof excitations

3.1.1 Description of example structure

In this study, a benchmark structure provided by the ASCE task group on structural health monitoring and damage detection (ASCE 2000, Johnson *et al.* 2000) was used to identify the modal parameters without input information. It is a 2-bay and 4-story building structure, which is a numerical model for a test frame at Univ. of British Columbia (Ventura *et al.* 1997) as shown in Fig. 1. The structure was subjected to roof excitations in x - and y -directions. 10 sets of acceleration data of 40 sec long were generated using the Acceleration Response Generation Program provided by the ASCE task group. The acceleration data were obtained with a sampling rate of 1000 Hz. Various levels of the measurement noise were considered to investigate the effect of the measurement noise, i.e. 0%, 20%, 40% and 60% in the root mean square (RMS) levels. Fig. 2 shows typical examples of the response time history at roof in x - and y -directions.

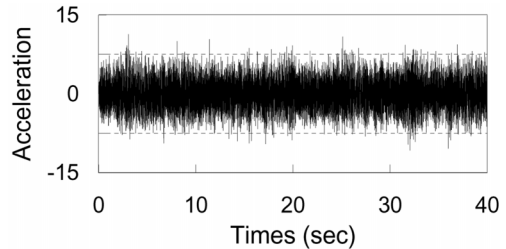


(a) UBC structure

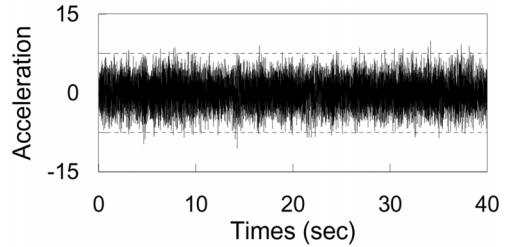


(b) Numerical model

Fig. 1 ASCE benchmark structure



(a) x-directional (15th sensor)



(b) y-directional (16th sensor)

Fig. 2 Acceleration time histories at the roof (cm/sec²)

3.1.2 Frequency domain methods

For frequency domain methods, FFT analyses were carried out using 4096 data points with a Hanning window and 50% overlapping. In the case of the PS method, two measurement data (at 15th and 16th sensors in *x*- and *y*-directions, respectively) on the roof were used as the referencing measurement points in two directions. Fig. 3 shows the PSD components at two sensors and the first singular value ($\sigma_1(\omega)$) of the PSD function matrix. It can be observed that each individual PSD function gives partial information on the natural frequencies, i.e. the component of 11 Hz is missing in $S_{y_{15}y_{15}}$, while the one of 9 Hz is missing in $S_{y_{16}y_{16}}$. However all components can be obtained from the first singular value ($\sigma_1(\omega)$), since all of the measured data were processed in the FDD method. It can be observed that the magnitudes of the PSD functions and first singular value are not the same, because most of the power in the measurement acceleration data was concentrated on the first singular value.

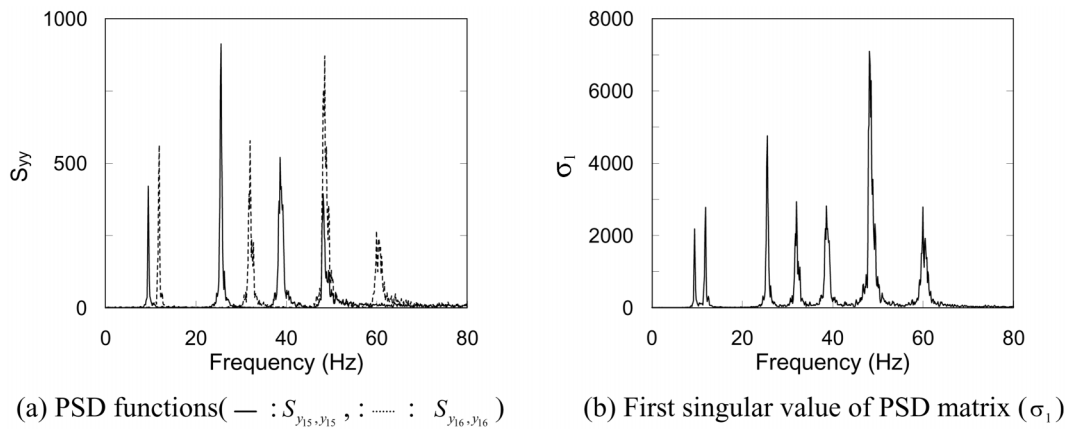


Fig. 3 PSD functions of the responses and its singular value

3.1.3 Time domain methods

For the ITD method, two measurement data at the 15th and 16th sensors on the roof were utilized as reference points in two directions as in the PS method. In the cases of the ITD and ERA methods, the cross-correlation functions were calculated to obtain the free vibration responses (James *et al.* 1996, Yam *et al.* 1997). Table 1 shows one of the most essential procedures in the ITD method to distinguish the real structural modes among many estimated modes. In the case of the ITD method, different modal parameters might be identified from the cases using different reference sensors, so many trivial modes may appear as shown in Table 1. In such situation, the modal confidence factor (MCF, Ibrahim 1978) can play an important role to distinguish the real structural modes. In this example, the modes in *x*-direction were identified using the 15th sensor as a reference sensor, while the modes in *y*-direction were estimated using the 16th sensor. If there are similar modes, the MCF value can be used to select the real structural modes. For example, in the case with the 15th sensor as the reference, both of the 12th and 13th identified natural frequencies are very similar, i.e. 60.12 Hz and 60.69 Hz, but the MCF value of the 12th mode is larger than the value of the 13th mode. Therefore, the 12th identified modal parameter can be selected as the 4th bending mode in *x*-direction (Bx4) even though there is just a very small difference between the MCF values of the 12th and 13th identified modes.

Table 1 Determination of real modes by ITD method: with 20% RMS noise

Estimated natural frequencies (Ref. Signal: 15)				Estimated natural frequencies (Ref. Signal: 16)			
No	MCF	Freq(Hz)	Index	No	MCF	Freq(Hz)	Index
1	0.9991	11.7567	Bx1	1	0.9985	9.4494	By1
2	0.9896	14.6538		2	0.9975	12.6553	
3	0.9883	28.0645		3	0.9969	25.5075	By2
4	0.9969	31.9643	Bx2	4	0.9077	32.4606	
5	0.9544	32.8436		5	0.9719	32.6640	
6	0.9534	38.8631		6	0.9961	38.6841	By3
7	0.9982	48.1083		7	0.9514	39.1053	
8	0.9989	48.6257	Bx3	8	0.8953	46.6978	
9	0.9631	51.3504		9	0.9968	48.0885	By4
10	0.8842	51.4968		10	0.8112	48.3362	
11	0.8681	57.1474		11	0.9987	48.6660	
12	0.9474	60.1154	Bx4	12	0.8575	53.3518	
13	0.9438	60.6881		13	0.9856	60.1079	
14	0.9299	61.5883		14	0.8024	61.5037	
15	0.8306	66.8176		15	0.6932	62.4923	

Fig. 4 shows the stabilization charts to identify the natural frequencies from the measured acceleration data with 60% measurement noises by the ERA, SSI/BR and SSI/CVA methods. There are 8 detectable modes for the ASCE benchmark structure, and all of those appear to be identified reasonably from the figures. However, in the case of the SSI/CVA, it is found that the modes can be more clearly identified than the other cases, since the SSI/CVA considers the canonical variety analysis to maximize the correlation between the measured data at different locations.

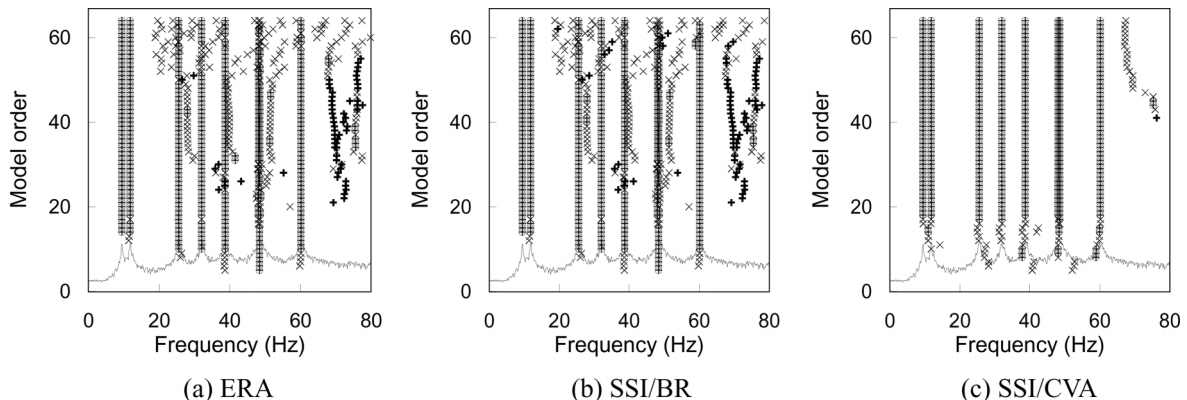


Fig. 4 Comparison of stabilization charts (\oplus : stable mode, $+$: unstable mode, \times : noise mode, $-$: 1st singular value $\sigma_1(\omega)$)

3.1.4 Comparisons of estimated results

Tables 2 and 3 show the identified modal parameters including the natural frequencies and modal damping ratios for the case of 20% measurement noise along with the exact values. Figs. 5 and 6 present comparisons of the errors estimated by several methods under various measurement noise levels. Figs. 7 and 8 show the estimated results of the mode shapes. Generally, the performances of the time domain methods are better than those of the frequency domain methods.

Between two frequency domain methods, the FDD method gives more accurate results than the PS method. In the case with 60% measurement noise, the maximum estimation error for the natural frequencies is about 0.4% in the PS method, while it is about 0.2% in the FDD method. In the case of the mode shapes shown in Figs. 7 and 8, the estimated mode shapes are very close to the exact mode shapes and their modal assurance criteria (MAC, Ewin 1984) values are above 0.99 for the isolated modes. But for the closely space modes such as the 6th and 7th modes (By4 and Bx3), the estimated mode shapes are quite corrupted and the MAC values reduced to a range of 0.4-0.9, since their modes are affected by each other. However the estimated results by the FDD method are found to be better than those by PS method. The damping ratios were not identified by the frequency domain methods, since the results by the frequency domain method are generally not reliable.

Among the time domain methods, the SSI/CVA method gives the best estimates. Estimation errors for the natural frequencies by the ITD are less than 0.4%, while those by the ERA, SSI/BR and SSI/CVA are less than 0.1%. The estimated modal damping ratio for the 1st mode by the ITD method has almost 200% error for the case with noise of 60%, however those by the ERA and SSI/BR are

Table 2 Estimated natural frequencies (Hz): with 20% RMS noise

Mode	Exact	Frequency Domain		Time Domain			
		PS	FDD	ITD	ERA	SSI/BR	SSI/CVA
By1	9.411	9.413	9.413	9.426	9.407	9.406	9.414
Bx1	11.791	11.773	11.773	11.776	11.792	11.792	11.800
By2	25.545	25.499	25.513	25.546	25.537	25.537	25.543
Bx2	32.006	32.023	32.023	32.017	31.997	31.997	32.007
By3	38.663	38.696	38.683	38.686	38.671	38.675	38.669
By4	48.007	48.164	48.096	47.962	47.947	47.945	47.964
Bx3	48.443	48.462	48.448	48.557	48.481	48.481	48.485
Bx4	60.151	60.289	60.181	60.154	60.163	60.162	60.133

Table 3 Estimated damping ratio (%): with 20% RMS noise

Mode	Exact	ITD	ERA	SSI/BR	SSI/CVA
By1	1.000	1.976	1.220	1.065	1.029
Bx1	1.000	1.048	0.871	1.096	0.969
By2	1.000	1.142	1.089	0.968	0.981
Bx2	1.000	1.038	1.046	1.035	1.005
By3	1.000	1.143	1.089	0.968	0.981
By4	1.000	1.038	1.048	1.030	1.003
Bx3	1.000	1.165	1.101	0.961	0.961
Bx4	1.000	1.017	1.020	1.009	1.032

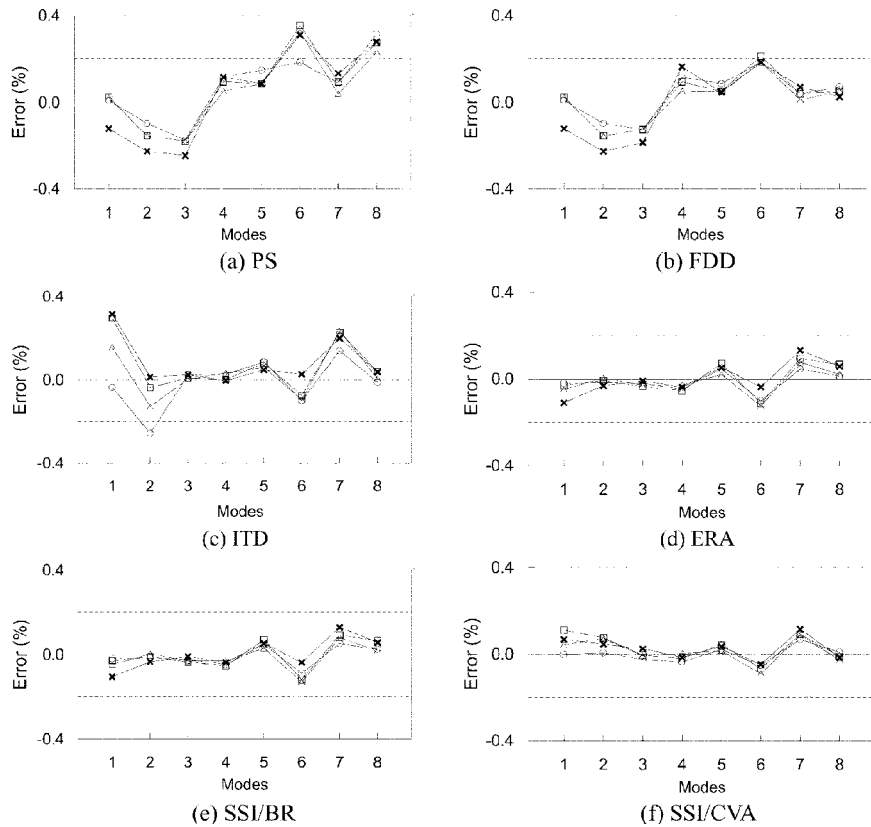


Fig. 5 Estimation errors of the natural frequencies for various methods (Noise levels with \circ : 0% \triangle : 20%, \square : 40%, \times : 60%)

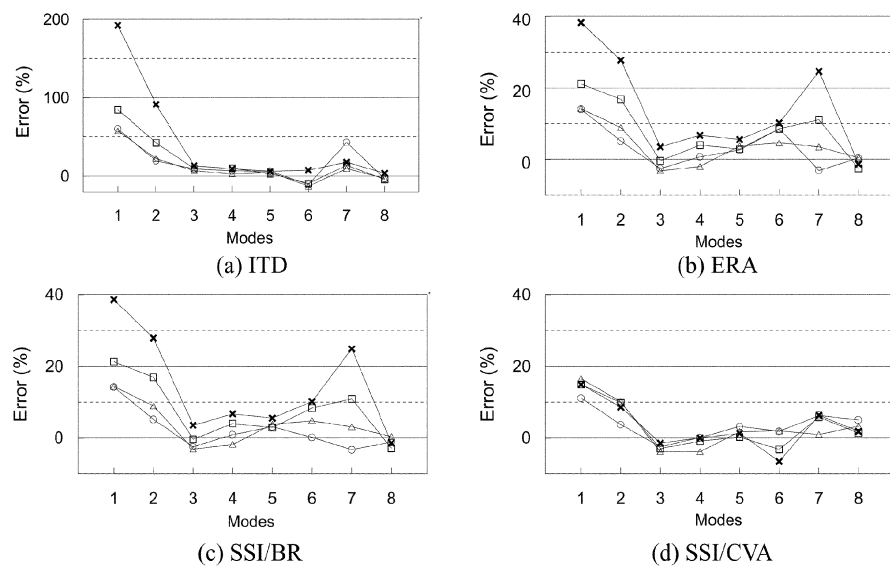


Fig. 6 Estimation errors of damping ratios for various methods (Noise levels with \circ : 0% \triangle : 20%, \square : 40%, \times : 60%)

less than 40%, and the errors by the SSI/CVA is under than 20%. In other word, the best results have been obtained by the SSI/CVA. For the case of the mode shapes, MAC values estimated by all the time domain methods are found to be over 0.96, even though some of them are closely spaced (By4 and Bx3).

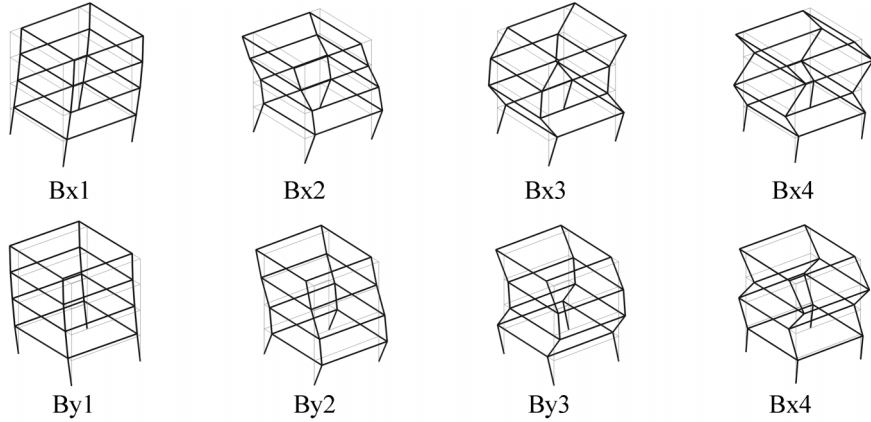


Fig. 7 Estimated mode shapes by SSI/CVA: case with 20% RMS noise

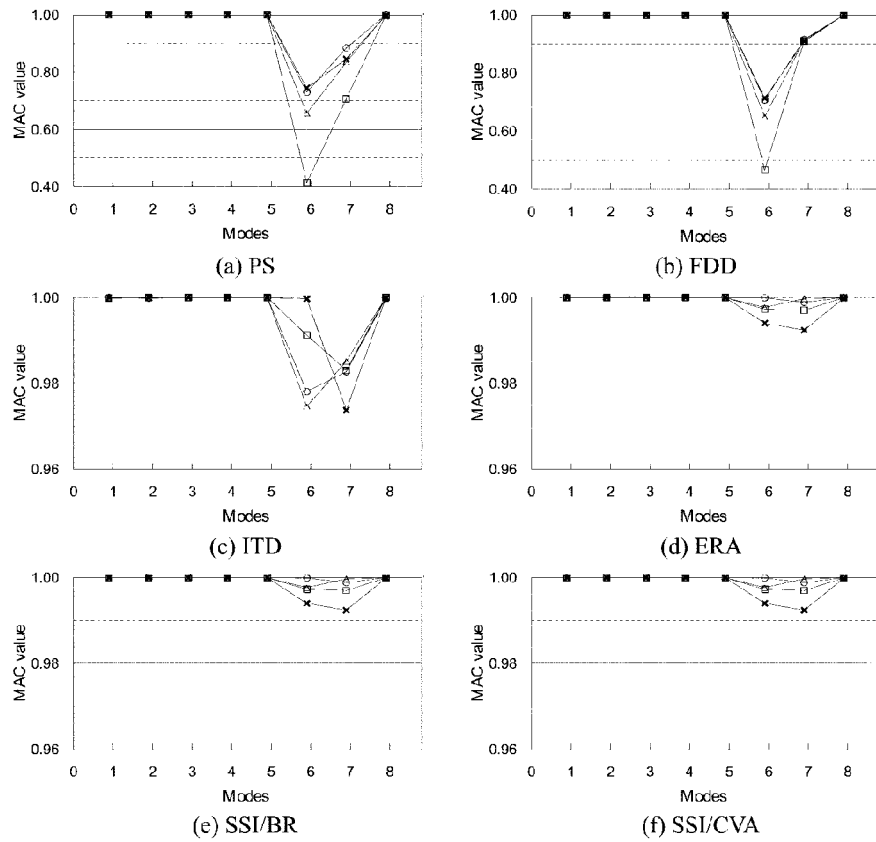


Fig. 8 MAC values by various methods (Noise levels with \circ : 0%, \triangle : 20%, \square : 40%, \times : 60%)

3.2 Example 2: NTU structure subjected to earthquake loadings

Modal identification was carried out on a 5 story steel frame structure tested on a shaking table in National Taiwan University (NTU) shown in Fig. 9 (Loh *et al.* 2000). Similar procedures to those in the ASCE benchmark structure were used. El Centro earthquake records with reduced peak accelerations (20% in *x*-dir and 30% in *y*-dir) and Kobe earthquake records with reduced peak accelerations (8% in *x*- and *y*-directions) shown in Fig. 10 were used, and the consistency of the estimates from the responses for two different inputs were examined. The present identifications

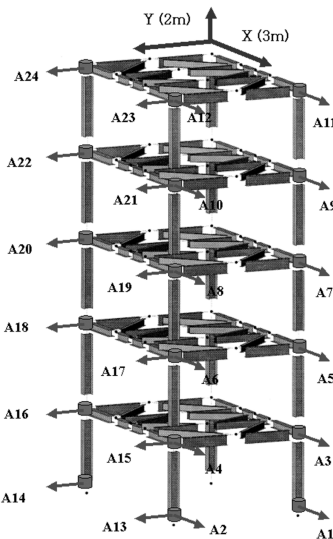


Fig. 9 NTU benchmark structure

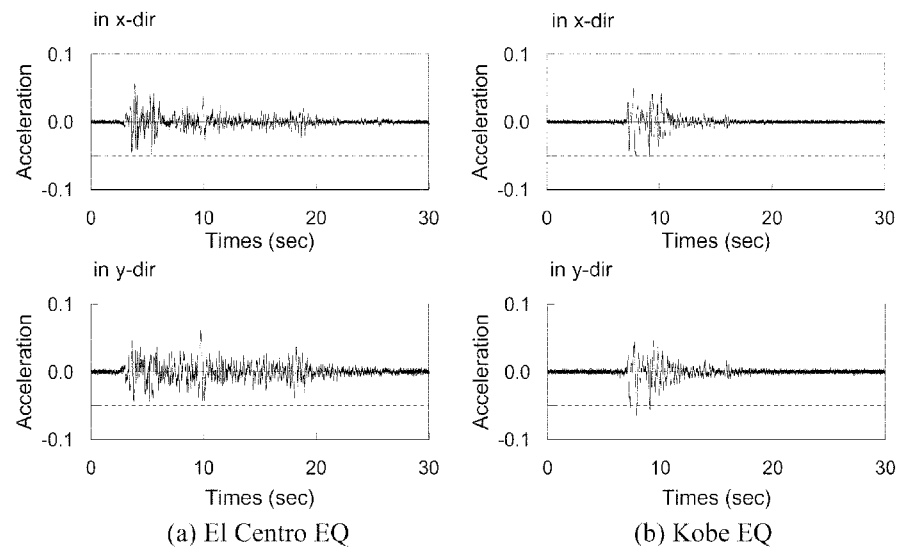


Fig. 10 Input ground accelerations

were carried out using only two sets of the response measurement data for different input excitations without using the input information at all.

The natural frequencies and modal damping ratios estimated for two cases with different earthquake excitations are summarized in Table 4. In Table 4, the values in the parentheses are modal damping ratios (%), and EC and KO stand for El Centro EQ and Kobe EQ, respectively. As far as the natural frequencies are concerned, it can be observed that the estimates are very consistent: i.e. the differences due to the different excitations are less than 1.5%, and those owing to the different methods are less than 4.0%. And it can be observed that the estimates are very close to the reference values identified by Loh *et al.* (2000). On the other hand, the estimates for modal damping ratios show relatively large discrepancy. For example, the modal damping ratio for the first x-dir bending mode is estimated as 1.3-2.8% for the case with El Centro EQ and 4.2-6.1% for the

Table 4(a) Estimated natural frequencies (Hz) and modal damping ratios (%): Bending modes in x-dir

Modes	EQ	PS	FDD	ITD	ERA	SSI/BR	SSI/CVA	Loh <i>et al.</i> (2000)
Bx1	EL	1.367	1.367	1.392(2.80)	1.390(1.72)	1.390(1.71)	1.400(1.39)	
	KO	1.367	1.367	1.338(4.19)	1.303(4.48)	1.303(4.47)	1.411(6.14)	1.40
Bx2	EL	4.492	4.492	4.510(0.77)	4.495(1.54)	4.495(1.54)	4.499(1.76)	
	KO	4.492	4.492	4.539(1.07)	4.547(0.63)	4.547(0.63)	4.531(0.63)	4.52
Bx3	EL	8.301	8.301	8.269(0.74)	8.242(0.75)	8.249(0.77)	8.233(0.76)	
	KO	8.203	8.203	8.208(0.83)	8.200(1.56)	8.199(1.56)	8.196(1.53)	
Bx4	EL	12.500	12.598	12.450(0.91)	12.424(0.83)	12.423(0.84)	12.395(0.69)	
	KO	12.402	12.695	12.411(0.79)	12.407(0.50)	12.407(0.50)	12.405(0.46)	
Bx5	EL	16.016	16.016	16.021(0.17)	16.018(0.22)	16.018(0.22)	16.009(0.22)	
	KO	16.016	16.016	16.035(0.23)	16.027(0.30)	16.027(0.30)	16.011(0.36)	
Difference Indices (%)		0.198	0.196	0.574(12.79)	0.832(32.34)	0.840(32.25)	0.204(37.62)	

Table 4(b) Estimated natural frequencies (Hz) and modal damping ratios (%): Bending modes in y-dir

Modes	EQ	PS	FDD	ITD	ERA	SSI/BR	SSI/CVA	Loh <i>et al.</i> (2000)
By1	EL	2.051	2.051	1.997(1.65)	2.062(3.46)	2.062(3.48)	2.074(3.33)	
	KO	2.246	2.246	2.160(4.12)	2.174(4.32)	2.173(4.32)	2.096(3.14)	2.14
By2	EL	6.836	6.836	6.854(0.12)	6.854(0.24)	6.854(0.24)	6.852(0.22)	
	KO	6.836	6.836	6.840(0.92)	6.866(0.89)	6.866(0.88)	6.866(1.03)	6.99
By3	EL	12.695	12.695	12.674(0.17)	12.674(0.12)	12.674(0.12)	12.672(0.12)	
	KO	12.695	12.109	12.678(0.18)	12.668(0.09)	12.668(0.09)	12.667(0.11)	
By4	EL	18.164	18.164	18.217(0.32)	18.247(0.35)	18.244(0.36)	18.231(0.15)	
	KO	18.164	18.164	18.153(1.31)	18.185(0.45)	18.191(0.44)	18.216(0.60)	
By5	EL	25.098	25.000	25.074(1.14)	25.136(0.78)	25.157(0.78)	25.167(0.69)	
	KO	25.098	25.098	25.171(1.08)	25.321(1.08)	25.322(1.08)	25.246(1.10)	
Difference Indices (%)		0.908	1.419	0.882(37.21)	0.658(22.30)	0.641(21.67)	0.169(31.00)	

Table 4(c) Estimated natural frequencies (Hz) and modal damping ratios (%): Torsional modes

Modes	EQ	PS	FDD	ITD	ERA	SSI/BR	SSI/CVA
T1	EL	3.516	3.516	3.529(0.16)	3.522 (0.21)	3.522 (0.20)	3.524 (0.39)
	KO	3.516	3.516	3.531(0.42)	3.530 (0.34)	3.530 (0.29)	3.535 (0.38)
T2	EL	11.426	11.426	11.436(0.41)	11.419(0.27)	11.419(0.27)	11.410(0.36)
	KO	11.426	11.426	11.426(0.23)	11.435(0.28)	11.436(0.28)	11.428(0.49)
T3	EL	21.191	21.191	21.150(0.20)	21.144(0.58)	21.174(0.58)	21.160(0.77)
	KO	21.191	21.191	21.234(0.46)	21.223(0.34)	21.215(0.27)	21.251(0.34)
T4	EL	32.031	32.031	31.985(0.80)	32.115(0.42)	32.117(0.42)	32.015(0.45)
	KO	32.129	32.129	32.179(0.26)	32.162(0.28)	32.162(0.28)	32.142(0.42)
T5	EL	42.090	40.430	40.645(3.72)	40.435(0.41)	40.434(0.41)	40.631(0.85)
	KO	40.723	40.625	40.645(1.24)	40.587(0.37)	40.594(0.35)	40.606(0.55)
Difference Indices (%)		0.361	0.079	0.115(42.66)	0.126(15.33)	0.110(16.91)	0.136(16.04)

Note¹⁾ Difference Index $(a, b) \triangleq |(a - b)/(a + b)| * 100(\%)$

Table 5 Comparison of MAC between estimated mode shapes using different inputs

Modes	PS	FDD	ITD	ERA	SSI/BR	SSI/CVA
Bx1	0.9671	0.9880	0.8830	0.9284	0.9278	0.9431
By1	0.9634	0.9559	0.9885	0.9883	0.9885	0.9923
T1	0.9715	0.9308	0.9942	0.9184	0.9267	0.9472
Bx2	0.9953	0.9916	0.9969	0.9949	0.9948	0.9929
By2	0.9989	0.9987	0.9991	0.9999	0.9999	0.9980
Bx3	0.9956	0.9905	0.9952	0.9883	0.9879	0.9908
T2	0.9596	0.9148	0.9772	0.9783	0.9780	0.9866
Bx4	0.6160	0.9175	0.8004	0.7316	0.7318	0.7536
By3	0.9996	0.9434	0.9881	0.9996	0.9996	0.9993
Bx5	0.9995	0.9990	0.9988	0.9990	0.9990	0.9952
By4	0.9517	0.8807	0.9600	0.9785	0.9755	0.9757
T3	0.9969	0.9835	0.9982	0.9961	0.9992	0.9974
By5	0.8958	0.8221	0.9101	0.9727	0.9759	0.9903
T4	0.9972	0.9931	0.9934	0.9987	0.9983	0.9986
T5	0.8465	0.9959	0.9429	0.9979	0.9978	0.9910
Mean	0.9436	0.9537	0.9617	0.9647	0.9654	0.9701

case with Kobe EQ. The large discrepancies of the estimated damping ratios in the lower frequency range may be caused by the different frequency contents of two excitations in this range.

The MAC values between two mode shapes estimated from two different excitations using El Centro EQ and Kobe EQ are larger than 0.95 for most of the cases, so it may be considered that the mode shapes have been reasonably estimated (see Table 5). However, the MAC values of the 4th bending mode in *x*-direction (Bx4) are less than those of the other modes. It may be caused by the fact that the Bx4 mode is very closely spaced with the By3 mode: i.e. those for the Bx4 and By3 modes are about 12.4-12.7 Hz and about 12.6-12.7 Hz, respectively.

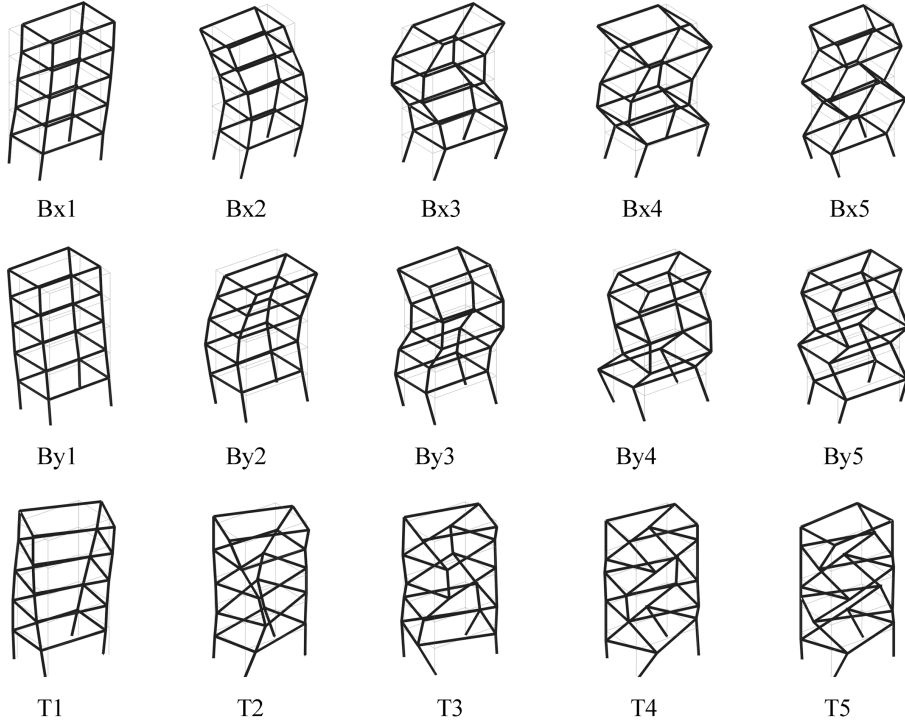


Fig. 11 Estimated mode shapes (SSI/CVA; EL Centro EQ)

3.3 Example 3: bridge model under traffic loadings

Fig. 12 shows a bridge model with a composite deck and vehicle models on it. The deck consists of two steel girders and a concrete slab. Accelerometers were installed along two girders as shown in Fig. 13. Ten (10) sets of round-trip tests were carried out using vehicle models, and the vertical acceleration responses were measured with a sampling rate of 1000 Hz for 30 sec (Lee *et al.* 2002).

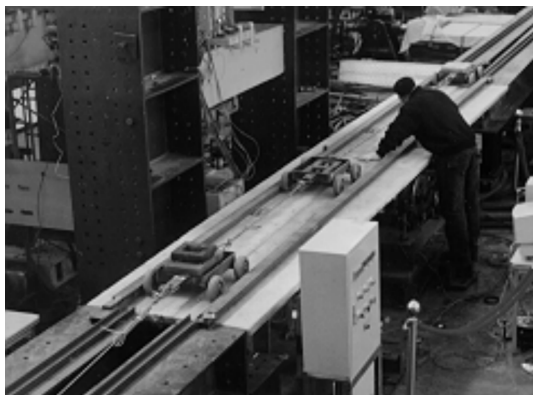


Fig. 12 Bridge model with traffic loading

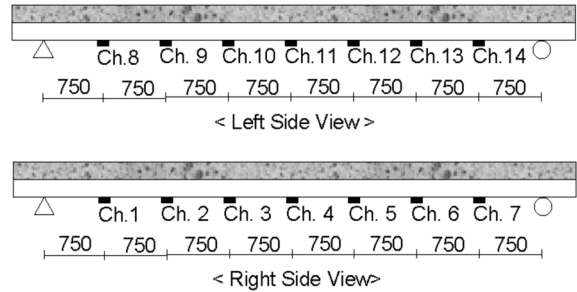


Fig. 13 Accelerometers on girders (unit:mm)

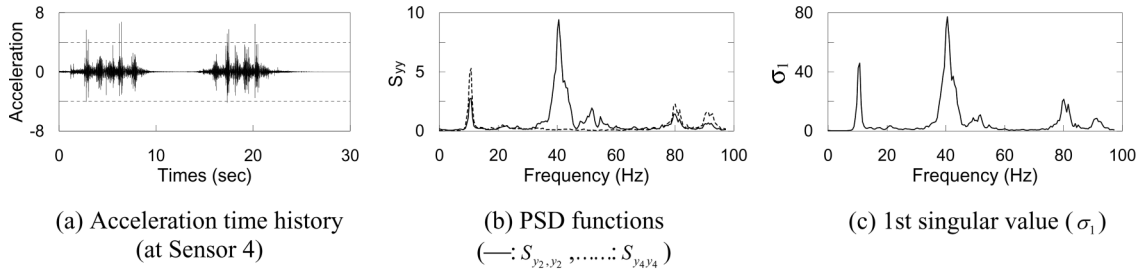


Fig. 14 Time history, PSD functions, and 1st singular value

Fig. 14(a) shows the typical acceleration time history of Sensor 4, and Figs. 14(b) and 14(c) show the PSD functions at Sensors 2 and 4, and the first singular value ($\sigma_1(\omega)$) of the PSD matrix.

By observing Fig. 14(b), the second bending mode (appeared near 40 Hz) is expected to be extracted well from the acceleration data at Sensor 2 using the PS method, while poorly from the data at Sensor 4, since the mode has a nodal point at Sensor 4 and the maximum amplitude at Sensor 2. However, all the modes can be identified from the FDD method since it utilizes the responses at all the sensors. From the PSD amplitude, it can be also expected that the 2nd bending mode around 40 Hz would be estimated most reliably, because the amplitude of the peak of the PSD is higher than the other peaks, which also means the 2nd bending mode was sufficiently excited by traffic loading. It can be verified by looking into the coefficient of variation (COV) values of the estimated results for 10 sets of test data particularly by the time domain methods.

Tables 6 and 7 summarize the estimated natural frequencies (Hz) and modal damping ratios (%), respectively, and the values in the parentheses in the tables are the COVs of the estimated results (%). The COVs of 10 natural frequencies estimated using each of the identification methods are found to be less than 3.4%, which means each method gives very consistent natural frequencies. The mean natural frequencies by each method are also very consistent. Among the results, those by the SSI/CVA are most consistent. However, the COVs of the estimated damping ratios are in the range of 10-52%. The discrepancies among the estimated damping from different methods are fairly big particularly for the first two modes.

Table 6 Means of estimated natural frequencies (Hz)

Modes	PS	FDD	ITD	ERA	SSI/BR	SSI/CVA	Lee <i>et al.</i> (2002)
B1	10.42(2.42)	10.42(2.42)	10.51(3.40)	10.14(0.71)	10.14(0.68)	10.46(0.39)	10.42
T1	21.57(0.92)	21.32(1.18)	20.87(1.36)	21.31(0.69)	21.30(0.67)	21.54(0.47)	
B2	40.53(0.76)	40.53(0.76)	40.61(0.12)	40.63(0.15)	40.62(0.15)	40.66(0.08)	40.47
T2	51.43(0.78)	51.51(0.52)	51.45(0.61)	51.52(0.57)	51.52(0.55)	51.67(0.30)	
B3	80.65(1.24)	81.14(0.89)	81.10(0.68)	81.41(0.61)	81.38(0.62)	81.04(0.41)	81.37
T3	91.23(0.53)	91.15(0.44)	91.08(0.17)	91.15(0.14)	91.15(0.13)	91.18(0.15)	
Mean of COV	1.11	1.03	1.06	0.48	0.47	0.30	

Table 7 Means of estimated modal damping ratios (%)

Modes	ITD	ERA	SSI/BR	SSI/CVA
B1	16.15(51.99)	2.56(45.78)	2.59(45.80)	14.17(31.96)
T1	28.59(24.70)	4.23(17.54)	4.24(17.93)	7.03(24.86)
B2	3.64(17.76)	4.01(15.88)	3.99(15.70)	3.95(15.05)
T2	3.97(19.55)	3.34(20.44)	3.34(20.93)	3.61(12.60)
B3	2.22(20.89)	2.11(15.40)	2.13(16.92)	2.39(9.77)
T3	1.83(15.57)	1.70(12.57)	1.70(12.63)	1.85(14.87)
Mean of COV	25.08	21.27	21.65	18.19

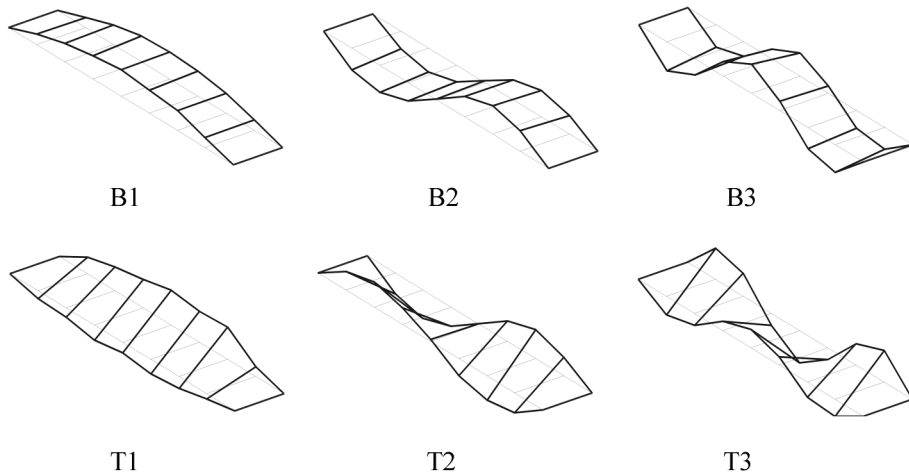


Fig. 15 Estimated mode shapes (SSI/CVA)

4. Conclusions

The following conclusions have been obtained on the modal parameter identification methods without input information through the numerical and experimental investigations on three example structures:

- (1) The frequency domain methods (PS and FDD) are generally more vulnerable to the measurement noise than the time domain methods (ITD, ERA, SSI/BR and SSI/CVA), and the estimates by the frequency domain methods are less accurate than those by time domain methods particularly when the two adjacent modes are closely spaced.
- (2) The FDD method is more attractive than the conventional PS method, since the FDD method requires no reference sensors and gives more accurate estimates.
- (3) The ITD can give reliable estimates even for the close modes, if the reference points for the cross-correlation functions are appropriately specified. The SSI/CVA method gives most accurate estimates under the large measurement noise. The ERA and SSI/BR methods may yield the estimates with a similar level of accuracy for the mode shapes and natural frequencies, but not for the modal damping ratios.

- (4) In general, the estimates using the various methods in this study are very good and consistent for the natural frequencies and the mode shapes, but those for the damping ratios are neither accurate nor consistent particularly under large measurement noise, such as 40 or 60% in the RMS level.
- (5) The techniques dealt in this study were originally developed under the assumption that the input excitation is a Gaussian white-noise random processes or the structure is under the free decaying. However, it has been found from the second and the third examples that the present methods can be reasonably applied to the cases with more general wide-band random excitation.
- (6) The ERA, SSI/BR, and SSI/CVA methods require larger computation time than the others, however the results are more reliable and accurate. The SSI/CVA is most time consuming, since it requires the SVD calculations three times. The FDD or ITD method may be used in the preliminary tests due to the computational efficiency and the reasonable accuracy, and then the ERA, SSI/BR, or SSI/CVA method may be used to enhance the estimates in the finalizing procedure.

Acknowledgements

This study was carried out under the financial support from Smart Infra-Structure Technology Center (SISTeC) which was established at Korea Advanced Institute of Science and Technology (KAIST) under the sponsorship from Ministry of Science and Technology (MOST) and Korea Foundation of Science and Technology (KOSEF). The authors would like to express their sincere appreciation to the ASCE Structural Health Monitoring study group and Professor Loh at National Taiwan University.

References

- ASCE Structural Health Monitoring Committee (2000), <http://wusceel.cive.wustl.edu/asce.shm/default.htm>.
- Bendat, J.S. and Piersol, A.G. (1993), *Engineering Applications of Correlation and Spectral Analysis*, John Wiley & Sons, New York, USA.
- Brinker, R., Zhang, L. and Andersen, P. (2000), "Modal identification from ambient response using frequency domain decomposition", *Proc. of 16th Int. Modal Analysis Conf.*, San Antonio, Texas, USA, 625-630.
- Ewins, D.J. (1984), *Modal Testing: Theory and Practice*, Research Studies Press Ltd., Brüel & Kjaer.
- Hermans, L. and Van Der Auweraer, H. (1999), "Modal testing and analysis of structures under operational conditions: Industrial applications", *Mechanical Systems and Signal Processing*, **13**(2), 193-216.
- Ho, B.L. and Kalman, R.E. (1966), "Effective construction of linear state-variable models from input/output data", *Regelungstechnik*, **14**, 545-548.
- Ibrahim, S.R. (1977), "Random decremental technique for modal identification of structures", *J. Spacecraft and Rockets*, **14**(11), 696-700.
- Ibrahim, S.R. (1978), "Modal confidence factor in vibration testing", *J. Spacecraft and Rockets*, **15**, 313-316.
- Ibrahim, S.R. and Mikulcik, E.C. (1977), "A method for the direct identification of vibration parameters from the free response", *Shock and Vibration Bulletin*, No.47, Part 4, 183-198.
- Ibrahim, S.R. and Pappa, R.S. (1982), "Large modal survey testing using the Ibrahim time domain identification technique", *J. Spacecraft and Rockets*, **19**(5), 459-465.
- James III, G.H. Carne, T.G. and Lauffer, J.P. (1996), "The Natural Excitation Technique (NExT) for modal

- parameter extraction from operating structures”, *The Int. J. of Analytical and Experimental Modal Analysis*, **10**(4), 260-277.
- Johnson, E.A., Lam, H.F., Katafygiotis, L.S. and Beck, J.L. (2000), “A benchmark problem for structural health monitoring and damage detection”, *Proc. of 14th ASCE Engineering Mechanics Conference (EM2000)*, Austin, Texas, May 21-24, 2000.
- Juang, J.N. and Pappa, R.S. (1985), “An eigensystem realization algorithm for modal parameter identification and model reduction”, *J. Guidance, Control and Dynamics*, AIAA, **8**(5), 620-627.
- Junag, J.N. (1994), *Applied System Identification*, Prentice Hall, Englewood Cliffs, New Jersey, USA.
- Lee, J.W., Lim, J.D., Yun, C.B., Yi, J.H. and Shim, J.M. (2002), “Health monitoring method for bridges under ordinary traffic loadings”, *J. Sound Vib.*, **257**(2), 247-264.
- Loh, C.H., Lin, C.Y. and Huang, C.C. (2000), “Time domain identification of frames under earthquake loadings”, *J. Eng. Struct.*, ASCE, **126**(7), 693-703.
- Newland, D.E. (1984), *An Introduction to Random Vibration and Spectral Analysis*, Longman.
- Otte, D., Van de Ponseele, P. and Leuridan, J. (1990), “Operational shapes estimation as a function of dynamic loads”, *Proc. of the 8th Int. Modal Analysis Conf.*, 413-421.
- Overschee V.P. and De Moor, B. (1996), *Subspace Identification for Linear Systems*, Kluwer Academic Publisher.
- Ventura, C.E., Prion, H.G.L., Black, C., Rezai, K.M. and Latendresse, V. (1997), “Modal properties of a steel frame used for seismic evaluation studies”, *15th Int. Modal Analysis Conf.*, Orlando, Florida.
- Yam, L.H., Leung, T.P., Li, D.B. and Xue, K.Z. (1997), “Use of ambient response measurements to determine dynamic characteristics of slender structures”, *Eng. Struct.*, **19**(2), 145-150.
- Yang, J.C.S., Chen, J. and Dagalakis, N.G. (1984), “Damage detection in offshore structures by the random decremental technique”, *J. Energy Resources Technology*, Transaction of ASME, **106**, 38-42.